

Molecular engineering of Mn(II) diamine diketonate precursors for the vapor deposition of manganese oxide nanostructures

Chiara Maccato,^[a] Lorenzo Bigiani,^[a] Giorgio Carraro,^[a] Alberto Gasparotto,^[a] Roberta Seraglia,^[b] Jiyeon Kim,^[c] Anjana Devi,^[c] Gloria Tabacchi,^{*,[d]} Ettore Fois,^[d] Giuseppe Pace,^[b] Vito Di Noto,^[e] and Davide Barreca^{*,[b]}

Abstract: Molecular engineering of Mn(II) diamine diketonate precursors is a key issue for their use in the vapor deposition of manganese oxide materials. In the present work, we focus on two closely related β -diketonate diamine Mn(II) adducts with different fluorine content in the diketonate ligands. The target compounds were synthesized by a simple procedure and, for the first time, thoroughly characterized by a joint experimental-theoretical approach, to understand the ligand influence on their structure, electronic properties, thermal behavior and reactivity. The target compounds are monomeric and exhibit a *pseudo*-octahedral coordination of the Mn(II) centers, with differences in their structure and fragmentation processes related to the ligand nature. Both complexes can be readily vaporized without premature side decompositions, a favorable feature for their use as precursors for chemical vapor deposition (CVD) or atomic layer

deposition (ALD) applications. Preliminary CVD experiments at moderate growth temperatures enabled to fabricate high purity, single-phase Mn₃O₄ nanosystems with tailored morphology, which hold a great promise for various technological applications.

Introduction

Manganese oxide nanomaterials are of considerable importance for many technological applications, thanks to their diversified structures and variety of appealing chemical and physical properties.^[1] In particular, Mn₃O₄, a mixed valence state oxide with a tetragonal structure, has received attention thanks to its durability, low cost and attractive performances for a variety of end-uses, spanning from (photo)catalysts,^[1a,b,2] to anodes of Li-ion batteries and pseudocapacitors,^[1b,2b,3] up to electrochromic systems,^[4] magnetic media,^[5] and gas sensors.^[1d,6] In this widespread context, the fabrication of Mn₃O₄ nanostructures with tailored morphology (nanoparticles, nanorods, nanofractals,...) has been performed by a variety of synthetic techniques, encompassing microwave irradiation, hydrothermal/solvothermal routes, chemical bath deposition, and chemical vapor deposition (CVD).^[1a,b,2a,2c,4-7] In particular, the latter processes, along with atomic layer deposition (ALD), are compatible with current processing standards, thanks to the capability of achieving *in-situ*, large area growth of thin films and nanostructured materials with controlled properties.^[8] In this regard, the development of suitable precursor compounds endowed with high volatility, thermal stability and clean decomposition pathways is a very challenging research area,^[9] which would ideally guide, in a 'molecular engineering' approach, the modulation of material properties in view of the desired functional applications.

So far, the most used CVD and ALD Mn precursors are mainly based on β -diketonate derivatives,^[1e,10] some of which suffer from poor shelf life and/or unfavorable thermal properties,^[9e] especially if containing Mn(II). In fact, Mn(II) complexes bearing unfluorinated β -diketonate ligands are reported to readily decompose into Mn(III) derivatives,^[10d,11] yielding a poor control on the product phase composition. As a consequence, the obtainment of single-phase Mn₃O₄ nanomaterials with controlled crystallinity and morphology^[12] requires the tailoring of β -diketonate compound properties at a molecular level. In this regard, the use of fluorinated ligands, like hfa (1,1,1,5,5,5-hexafluoro-2,4-pentanedionate), is favorable for the obtainment of metal complexes with improved shelf-life, thermal and mass transport properties if compared to non-fluorinated compounds.^[9e] The hfa ligand bears two -CF₃ groups, which enhance volatility through the decrease of Van der

[a] Prof. C. Maccato, Dr. L. Bigiani, Dr. G. Carraro, Prof. A. Gasparotto, Department of Chemistry, Padova University and INSTM 35131 Padova, Italy

[b] Dr. R. Seraglia, Dr. G. Pace, Dr. D. Barreca CNR-ICMATE and INSTM, Department of Chemistry, Padova University 35131 Padova, Italy
E-mail: davide.barreca@unipd.it

[c] Dr. J. Kim, Prof. A. Devi Inorganic Materials Chemistry, Faculty of Chemistry and Biochemistry, Ruhr-University Bochum 44801 Bochum, Germany

[d] Prof. G. Tabacchi, Prof. E. Fois Department of Science and High Technology University of Insubria and INSTM 22100 Como, Italy
E-mail: gloria.tabacchi@uninsubria.it

[e] Prof. V. Di Noto Department of Industrial Engineering, Chemical Technology Section, in Department of Chemistry, Padova University and INSTM 35131 Padova (PD), Italy

Supporting information for this article is available on the www under <http://dx.doi.org/10.1002/chem>. It contains experimental crystallographic data and calculated parameters for MnL₂*TMEDA (Tables S1-S2), NBO charges and bond orders (Tables S3-S4), calculated structures of Mn-containing fragments (Figure S1), components of the π - π^* ligand-to-ligand transitions calculated for MnL₂*TMEDA (Figures S2-S3), molecular orbitals involved in the π - π^* electronic transitions calculated for the isolated hfa and tf ligands (Figure S4), MnL₂*TMEDA bond distances, stabilization energies and dipole moments in the presence of an electric field (Table S5), MS² and MS³ mass spectra of selected ions (Figures S5-S7), calculated structures of [Mn(hfa)₃]⁻ and [Mn(tf a)₃]⁻ ions (Figure S8). XPS data on a representative Mn₃O₄ specimen (Figure S9).

Waals intermolecular forces^[10d] and result in an enhanced Lewis acidity of the metal center,^[9e] enabling the effective binding of diamine Lewis bases like TMEDA (TMEDA = *N,N,N',N'*-tetramethylethylenediamine). The introduction of the latter enables a complete saturation of the metal coordination sphere, yielding β -diketonate-diamine compounds with general formula $M(\text{hfa})_2\cdot\text{TMEDA}$, which feature a higher stability towards hydrolysis and provide improved thermal/mass transport properties,^[13] important characteristics for their use as CVD precursors.

In our previous studies, we have devoted our attention on $M(\text{hfa})_2\cdot\text{TMEDA}$ complexes of various elements, in particular Cu,^[13a,14] Co,^[13b] Fe^[15] and Zn.^[16] Although all these molecular systems present a common structural motif, *i.e.* a pseudo-octahedral MO_4N_2 geometry, their investigation evidenced that the specific chemico-physical properties, as well as the features of the obtained CVD products, significantly depend on the nature of the metal center. Even in the case of manganese, stable Mn(II) compounds can be obtained using fluorinated diketonate ligands, such as hfa.^[9e,11,17] Now, the question arises as to whether the presence of only one $-\text{CF}_3$ group for each diketonate could be sufficient to endow the diamine adducts with the stability, volatility, and clean decomposition properties required for CVD/ALD applications. If the complex weakest bonds, *i.e.* the first to be broken, certainly depend on the metal center,^[14b,15c,16] the effect of the ligands is indeed equally important. Note that a diketonate with a single $-\text{CF}_3$ (indicated hereafter as tfa = 1,1,1-trifluoro-2,4-pentanedionate) could be formally obtained by replacing one of the hfa fluorinated moieties with a methyl group. How would such a ligand modify the chemistry of these precursors, and to what extent would their CVD performances be affected? Literature, unfortunately, offers no clear answer to these questions. Despite $M(\text{tfa})_2$ complexes have been reported for $M = \text{Co}$,^[18] Ni,^[19] Cu,^[20] $M(\text{tfa})_2\cdot\text{TMEDA}$ adducts have been much less studied than their hfa-containing counterparts. In fact, only a work mentioning $\text{Cu}(\text{tfa})_2\cdot\text{TMEDA}$ ^[21] is available so far and no direct connections between ligand properties and precursor behavior have been investigated in detail.

To elucidate such interrelations, we investigate herein the structure/property interplay for two Mn(II) complexes bearing either hexafluorinated or trifluorinated diketonate ligands, namely $\text{Mn}(\text{hfa})_2\cdot\text{TMEDA}$ and $\text{Mn}(\text{tfa})_2\cdot\text{TMEDA}$. It is worthwhile noticing that, despite the preparation of $\text{Mn}(\text{hfa})_2\cdot\text{TMEDA}$ has already been reported,^[22] only some data on its structure and thermal behavior are available in the literature,^[11,17] whereas a detailed theoretical-experimental characterization for this compound is completely missing. The need of these studies is even more relevant for $\text{Mn}(\text{tfa})_2\cdot\text{TMEDA}$, which, so far, has been mentioned only once in a patent as antiknock additive.^[22]

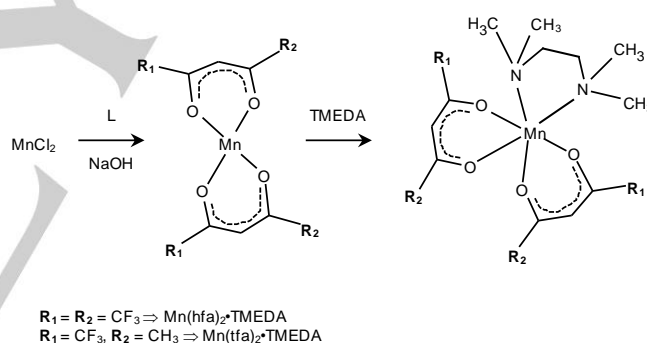
In this work, our main aim is to disclose how the ligand fluorination degree in $\text{MnL}_2\cdot\text{TMEDA}$ precursors affects their chemico-physical features, including stability, volatility and gas-phase fragmentation, with particular attention to their performances in the CVD of Mn_3O_4 nanomaterials. The experimental results presented herein for the two complexes are validated and integrated by a detailed DFT modeling, aimed at providing a theoretical basis^[23] for the interpretation of similarities and differences in their structure, bonding and chemical behavior. Finally, preliminary data concerning the low-pressure CVD validation of both compounds as

Mn molecular sources for high purity Mn_3O_4 nanodeposits on different substrates are also reported.

Results and Discussion

Synthesis and characterization of $\text{MnL}_2\cdot\text{TMEDA}$ compounds

In this work, the $\text{MnL}_2\cdot\text{TMEDA}$ adducts were synthesized through a procedure different from that reported in the literature for $\text{Mn}(\text{hfa})_2\cdot\text{TMEDA}$,^[17] involving the reaction in aqueous mixtures between Mn(II) chloride and L ligands in the presence of TMEDA (Scheme 1). The process, carried out at room temperature with no need of refluxing, at variance with a previous study,^[11] yielded the target adducts, that could be readily manipulated in the presence of air, moisture and light without any detrimental degradation. Beside a shelf-life of various months, an important feature for CVD applications, the present $\text{MnL}_2\cdot\text{TMEDA}$ compounds possessed an appreciable volatility (m.p. = 86 and 99°C for L = hfa and tfa, respectively^[22]) and could be readily sublimed under vacuum ($\approx 10^{-3}$ mbar). The melting point of $\text{Mn}(\text{hfa})_2\cdot\text{TMEDA}$ at atmospheric pressure was higher than that previously obtained by some investigators,^[11,17] but in line with that reported in a patent quoting the use of this compound as a gasoline additive.^[22]



Scheme 1. The synthesis of $\text{MnL}_2\cdot\text{TMEDA}$ derivatives.

The molecular structures of the two complexes are displayed in Figure 1, whereas crystallographic and structural refinement data, as well as geometrical parameters of DFT-calculated structures, are presented in Tables S1 and S2 in the Supporting Information. Selected bond lengths and angles are listed in Table 1. At variance with other cases, such as that of Mn bis(*N,N*-diisopropylacetamidinate)^[24] or variously substituted dialkylmanganese(II) complexes,^[8d] both compounds were monomeric both in the solid state and in solution [see also below for Electrospray Ionization-Mass Spectrometry (ESI-MS) results], indicating that the use of TMEDA was effective in saturating the Mn(II) coordination sphere. In addition, despite the synthesis was carried out in aqueous mixtures, no water molecules were present in the Mn(II) environment, and no classical hydrogen bonds occurred in the solid state structure. The latter feature is of key importance in view of CVD/ALD utilization^[13,15a] (see also below for thermoanalytical data). In contrast, for $\text{Mn}(\text{hfa})_2\cdot 2\text{H}_2\text{O}$ ^[10d] and other

FULL PAPER

Mn(II) β -diketonates like the adducts of Mn(hfa)₂ with substituted nitronyl nitroxides,^[25] the occurrence of hydrogen bonding has been observed.

In both cases of Figure 1, X-ray crystal structure determination provided evidence for a *cis* geometry,^[26] as also reported for

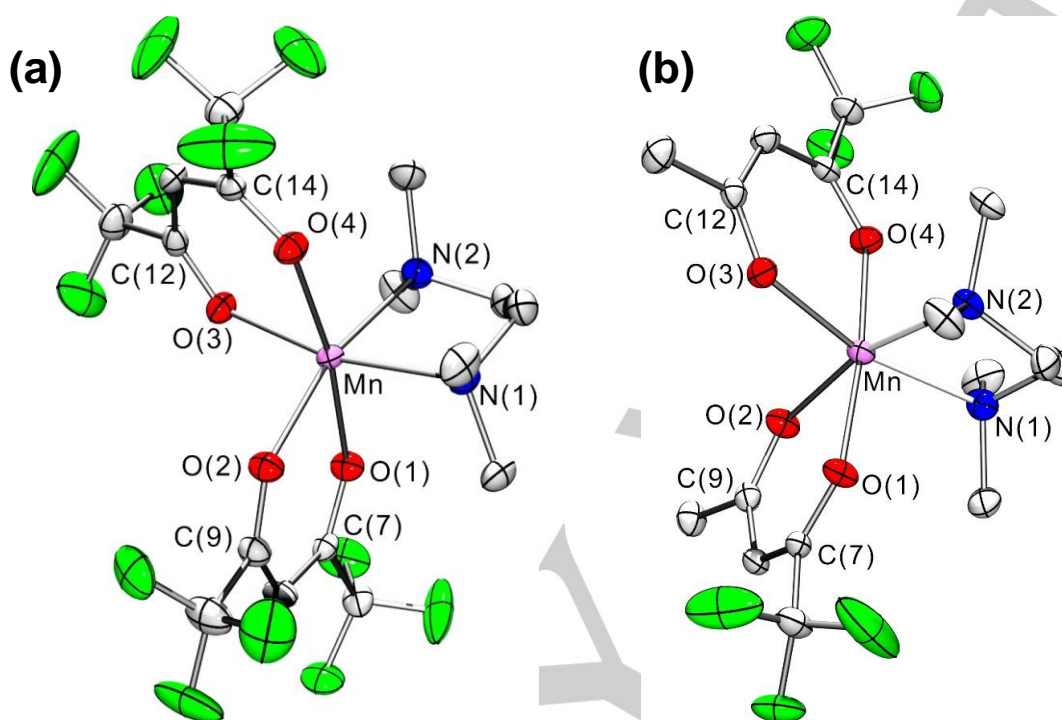


Figure 1. Molecular structures of (a) Mn(hfa)₂·TMEDA and (b) Mn(tfa)₂·TMEDA. Displacement ellipsoids are shown at the 50% probability level. Hydrogen atoms and rotational disorder from –CF₃ groups are omitted for clarity.

M(hfa)₂·TMEDA with M = Fe,^[15a] Co^[13b] and Cu,^[13a] with a two-fold axis bisecting the TMEDA ligand. Irrespective of the used β -diketonate, the mean Mn–O and Mn–N bond lengths were in agreement with those obtained for coordination complexes of 2-(4-quinolyl)nitronyl nitroxide^[27] and 2,2'-bipyridine^[28] with Mn(hfa)₂ and for various Mn(II)-hfa compounds, including Mn(hfa)₂·TMEDA,^[9e,10d,17,26] although the present work contains a better quality of structure refinement for the latter complex. As can be observed in Figure 1, both compounds presented a six-fold coordination around Mn(II) centers, resulting in a MnO₄N₂ distorted octahedral environment, in line with previous reports for homologous complexes available in the Cambridge Structural Database.^[26] In comparison to other ML₂·TMEDA adducts (M = Fe,^[15a] Co,^[13b] Cu,^[13a] Zn^[29]), the O–M–O, O–M–N, and N–M–N bond angles (Table 1) are slightly lower (up to $\approx 5^\circ$), whereas M–O and M–N distances are longer. Similarly to the Fe homologue,^[15a] the O–C bond lengths of β -diketonate ligands were all close to 1.25 Å, a value suggesting a double bond character (typical O–C single bonds ≈ 1.40 Å). For both compounds, the atomic distances between O(1)–C(7) and O(4)–C(14) are slightly longer than those of O(2)–C(9) and O(3)–C(12), due to the CF₃– electron withdrawing groups directly bonded to C(7) and C(14) atoms. In addition, Mn–O(2) and Mn–O(3) distances were slightly longer than those *trans* to the O atoms of L ligands [Mn–O(1) and Mn–O(4); compare the pertaining values, Table 1^[9e]]. A similar *trans* effect

has already been observed for M(hfa)₂·TMEDA compounds with M = Mg,^[30] Fe,^[15a] Co,^[13b] Zn.^[16,29] Finally, it is worth noting that, for both complexes, Mn–N bonds were longer than Mn–O ones. This effect, particularly evident for Mn(tfa)₂·TMEDA, anticipated an easier opening of the TMEDA

Table 1. Selected bond lengths and angles for Mn(hfa)₂·TMEDA and Mn(tfa)₂·TMEDA.

| Bond lengths (Å) | Mn(hfa) ₂ ·TMEDA | Mn(tfa) ₂ ·TMEDA |
|------------------|-----------------------------|-----------------------------|
| Mn–O(1) | 2.1472(14) | 2.1481(14) |
| Mn–O(2) | 2.1743(14) | 2.1629(14) |
| Mn–O(3) | 2.1546(14) | 2.1525(14) |
| Mn–O(4) | 2.1493(14) | 2.1265(14) |
| Mn–N(1) | 2.2984(17) | 2.3428(18) |
| Mn–N(2) | 2.2989(17) | 2.3116(17) |
| O(1)–C(7) | 1.251(2) | 1.261(2) |
| O(2)–C(9) | 1.245(2) | 1.255(2) |
| O(3)–C(12) | 1.244(3) | 1.252(2) |
| O(4)–C(14) | 1.248(3) | 1.260(2) |
| Bond angles (°) | | |
| O(1)–Mn–O(2) | 82.07(5) | 83.21(6) |
| O(3)–Mn–O(4) | 82.60(5) | 83.52(6) |
| N(1)–Mn–N(2) | 79.81(6) | 78.66(6) |

FULL PAPER

| | | |
|---------------|------------|------------|
| O(1)-Mn-O(4) | 171.03(5) | 173.85(6) |
| O(3)-Mn-N(1) | 167.48(5) | 166.57(6) |
| O(2)-Mn-N(2) | 166.34(6) | 166.49(6) |
| Mn-O(1)-C(7) | 130.02(13) | 127.70(13) |
| Mn-O(2)-C(9) | 129.06(13) | 130.70(13) |
| Mn-O(3)-C(12) | 128.78(13) | 131.12(13) |
| Mn-O(4)-C(14) | 129.13(13) | 127.72(13) |

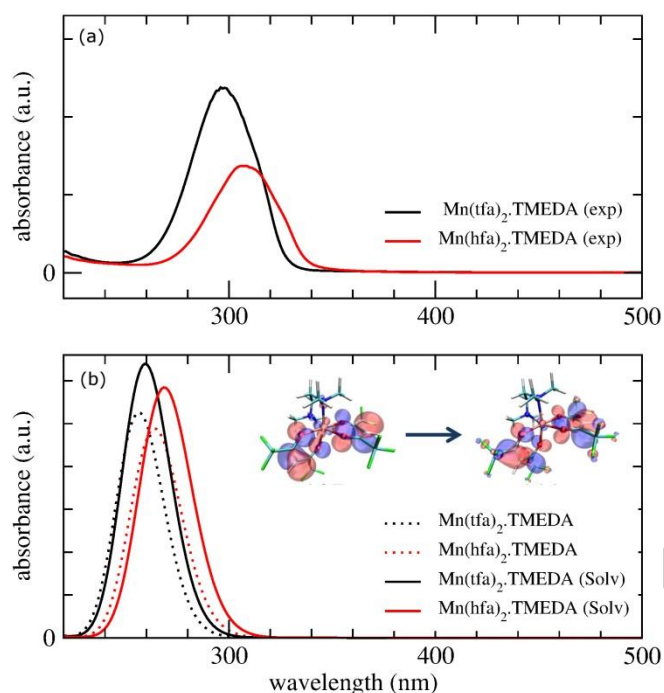


Figure 2. Experimental (a) and theoretical (b) UV-Vis optical spectra for $\text{Mn}(\text{hfa})_2\cdot\text{TMEDA}$ (red lines) and $\text{Mn}(\text{tfa})_2\cdot\text{TMEDA}$ (black lines). The orbitals involved in one of the components of the transition for $\text{Mn}(\text{hfa})_2\cdot\text{TMEDA}$ are shown in the inset of (b) (see Figures S2-S3 in the Supporting Information for graphical representations of all the components for the two complexes). Theoretical spectra were calculated both in vacuum (no label) and with a polarizable continuum model^[31] for the solvent ethanol (label 'Solv').

ring with respect to the β -diketonate one, as suggested by the calculated bond orders, electronic population analyses and decomposition energies for the two precursors. In both complexes, especially for $\text{Mn}(\text{tfa})_2\cdot\text{TMEDA}$, the diketonate is a stronger electron donor towards Mn if compared to the diamine (Table S3 in the Supporting Information). Accordingly, Mn-N bonds are significantly weaker than Mn-O ones (Table S4 in the Supporting Information), suggesting that, at least in the gas phase, the TMEDA ligand should be more easily released than the diketonate one. On this basis, we calculated the precursor decomposition energy (ΔE) for the following pathways [equations (1) and (2), with L=hfa/tfa] in vacuum and in methanol, *i.e.* the solvent used in the present ESI-MS experiments:



The geometries of $\text{MnL}\cdot\text{TMEDA}^+$ and MnL_2 fragments were initially optimized in vacuum. The loss of one ligand strongly desaturates

the Mn coordination sphere, and all fragments exhibit a tetrahedral coordination, as depicted in Figure S1 in the Supporting Information. For L = hfa, calculations yielded $\Delta E_1 = 125.4 \text{ kcal}\cdot\text{mol}^{-1}$ and $\Delta E_2 = 38.0 \text{ kcal}\cdot\text{mol}^{-1}$, whereas the corresponding values for L = tfa were $\Delta E_1 = 131.3 \text{ kcal}\cdot\text{mol}^{-1}$ and $\Delta E_2 = 31.0 \text{ kcal}\cdot\text{mol}^{-1}$. Hence, in the gas phase, the loss of a hfa/tfa moiety would be significantly unfavored with respect to the loss of TMEDA, in line with the previously discussed data. Nevertheless, when the same quantities are calculated in methanol,^[31] the difference substantially decreases, indicating that the energies involved in the two decomposition routes become comparable. This is particularly evident for L = hfa, where $\Delta E_1 = 30.3 \text{ kcal}\cdot\text{mol}^{-1}$ and $\Delta E_2 = 28.8 \text{ kcal}\cdot\text{mol}^{-1}$, while for L = tfa we found $\Delta E_1 = 32.9 \text{ kcal}\cdot\text{mol}^{-1}$ and $\Delta E_2 = 23.3 \text{ kcal}\cdot\text{mol}^{-1}$. The reaction medium plays therefore a key influence on fragmentation pathways. Fragmentation route (1), highly unfavored in vacuum, becomes viable in a polar solvent due to the stabilization of the resulting ionic species. This might be particularly important for ESI-MS experiments, where the first complex fragmentation occurs in the solvent (see below). On the other hand, route (2) should be favored in the gas-phase, such as in thermal CVD experiments.

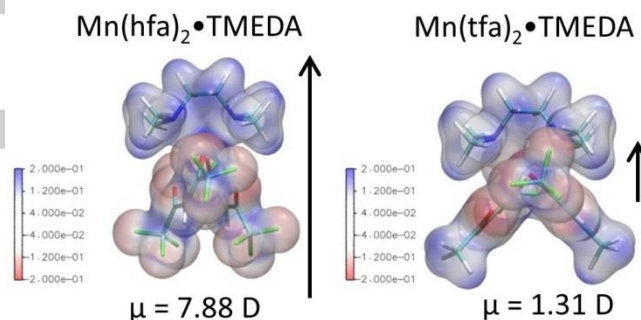


Figure 3. Electrostatic potential map for $\text{Mn}(\text{hfa})_2\cdot\text{TMEDA}$ and $\text{Mn}(\text{tfa})_2\cdot\text{TMEDA}$. Regions of high (positive) potential (in blue) are electron-poor, whereas regions of low (negative) potential (in red) are electron-rich. White/grey colors represent intermediate electrostatic potential values. Arrows mark the direction and magnitude of electric dipole moments μ . Atom color codes: Mn = pink; F = green; O = red; N = blue; C = cyan; H = white.

UV-Vis optical spectra of the compound are displayed in Figure 2. The broad band at $\lambda \approx 300 \text{ nm}$, due to electronic states mostly localized on the diketonate ligands (see inset in Figure 2b), arises from $\pi-\pi^*$ ligand-to-ligand excitations (see Figures S2-S4 in the Supporting Information). The calculated spectra reproduce the experimental trend, with a spectral shift to higher wavelengths for $\text{Mn}(\text{hfa})_2\cdot\text{TMEDA}$ compared to $\text{Mn}(\text{tfa})_2\cdot\text{TMEDA}$, and the agreement is further improved taking into account the solvent contribution. The same trend is found for the $\pi-\pi^*$ transitions in isolated hfa and tfa (see Figure S4 in the Supporting Information), indicating that the compound electronic excitation and optical properties are significantly influenced by the ligand nature.

This finding prompted us to investigate more closely the ligand effect on the electronic structures and electric dipole moments of the complexes. The results showed that $\text{Mn}(\text{hfa})_2\cdot\text{TMEDA}$ has a dipole moment considerably larger than $\text{Mn}(\text{tfa})_2\cdot\text{TMEDA}$, due to the net charge separation between hfa and diamine ligands, as

FULL PAPER

depicted in the electrostatic potential maps (Figure 3). Indeed, whereas the electrostatic potentials of TMEDA and hfa are respectively positive and negative, the tfa ligand exhibits both positive and negative regions, localized on the $-\text{CH}_3$ and $-\text{CF}_3$ groups, respectively. Hence, the application of external electric fields, as in ESI-MS experiments (see below), might have different effects on the two compounds. Calculations indicated that both complexes were slightly stabilized by a moderate electric field and showed a slight dipole moment increase, especially in the case of $\text{Mn}(\text{hfa})_2 \cdot \text{TMEDA}$ (see Table S5 in the Supporting Information). Such an electric field would therefore favor a preferential orientation of the complexes, with an enhanced effect for $\text{Mn}(\text{hfa})_2 \cdot \text{TMEDA}$ due to its more asymmetric charge distribution (Figure 3).

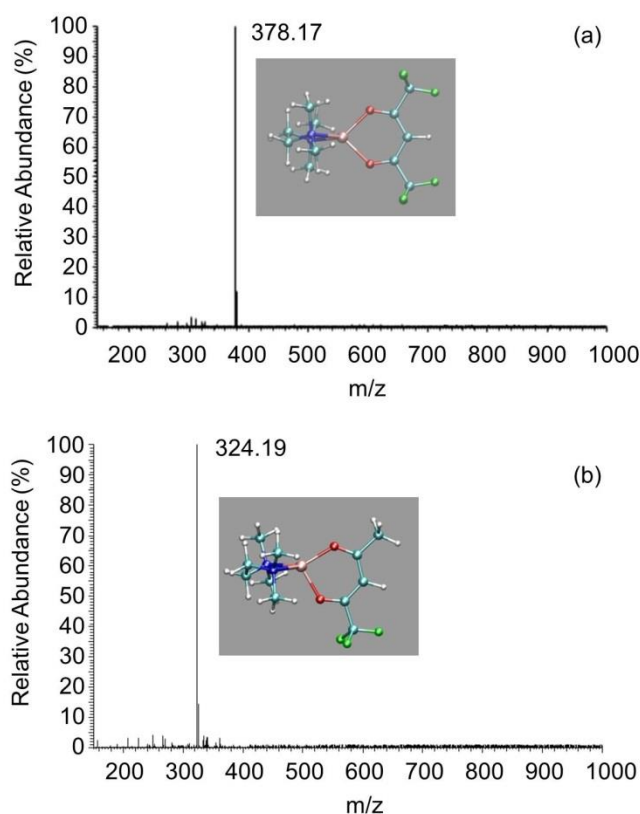


Figure 4. Positive ion ESI-MS spectra of (a) $\text{Mn}(\text{hfa})_2 \cdot \text{TMEDA}$ and (b) $\text{Mn}(\text{tfa})_2 \cdot \text{TMEDA}$ methanolic solutions. Calculated optimized structures for the most abundant ionic species are shown as insets. Atom color codes as in Figure 3.

An additional insight into the behavior of the two Mn complexes was obtained by means of ESI-MS, a soft ionization technique providing important clues on the compound reactivity. ESI-MS analyses were carried out in both positive (+) and negative (-) ion modes, with the aim of elucidating the adduct fragmentation pathways and their interplay with molecular structures. It is worthwhile observing that, to the best of our knowledge, no such investigation on $\text{MnL}_2 \cdot \text{TMEDA}$ compounds has ever been reported

in the literature up to date.

In positive ion mode, the behavior of the two compounds was qualitatively similar, irrespective of the ligand nature. ESI(+) mass spectra (Figure 4) are in fact dominated by single peaks centered at m/z 378 and 324, corresponding to $[\text{Mn}(\text{hfa}) \cdot \text{TMEDA}]^+$ and $[\text{Mn}(\text{tfa}) \cdot \text{TMEDA}]^+$, respectively. This result agreed with those previously obtained for analogous $\text{M}(\text{hfa})_2 \cdot \text{TMEDA}$ compounds, with $\text{M} = \text{Cu}$ and Co .^[13-14]

To attain a deeper insight into the complex fragmentation pathways, MS^2 and MS^3 experiments were carried out on $[\text{MnL} \cdot \text{TMEDA}]^+$ ions (see Figures S5-S6 in the Supporting Information). Irrespective of the ligand nature, MS^2 spectra were characterized by the presence of ions at m/z 190 and 115 corresponding to diamine-related derivatives, with the first one arising from a ligand-to-metal fluorine transfer process. This behavior was directly dependent on the metal nature, since similar MS^2 experiments on $[\text{M}(\text{hfa}) \cdot \text{TMEDA}]^+$ ions yielded $[\text{CuTMEDA} - \text{H}]^+$, for the Cu derivative,^[13a,14a] and $[\text{CoF}_2 \cdot \text{TMEDA} + \text{H}]^+$, for the Co one.^[13b]

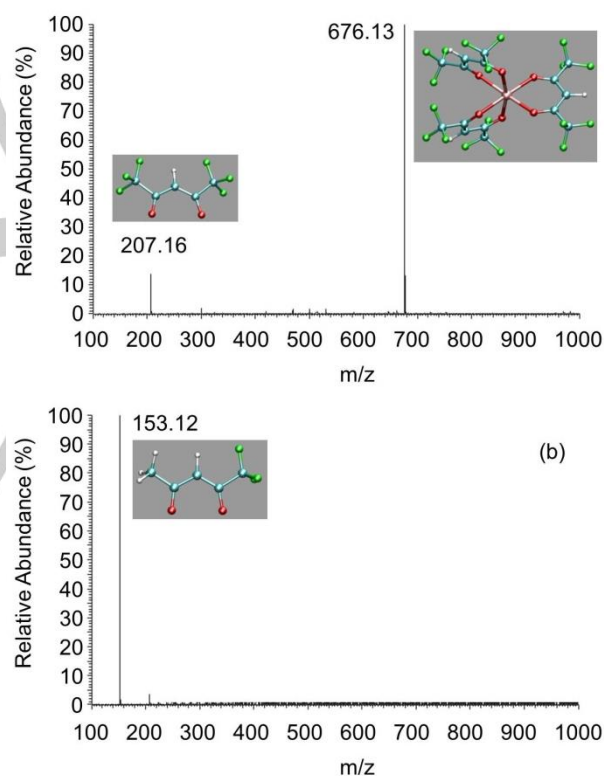


Figure 5. Negative ion ESI-MS spectra of (a) $\text{Mn}(\text{hfa})_2 \cdot \text{TMEDA}$ and (b) $\text{Mn}(\text{tfa})_2 \cdot \text{TMEDA}$ methanolic solutions. Calculated optimized structures for the most abundant ionic species are shown as insets. Atom color codes as in Figure 3.

In negative ion mode, $\text{MnL}_2 \cdot \text{TMEDA}$ ESI-MS spectra revealed a different influence of hfa/tfa ligands on the fragmentation pathway. ESI(-) mass spectrum of $\text{Mn}(\text{hfa})_2 \cdot \text{TMEDA}$ (Figure 5a) was characterized by the presence of ions at m/z 676 and 207, corresponding to $[\text{Mn}(\text{hfa})_3]^-$ and $[\text{hfa}]^-$, respectively. Conversely, the corresponding spectrum of $\text{Mn}(\text{tfa})_2 \cdot \text{TMEDA}$ (Figure 5b) displayed only the signal at m/z 153, corresponding to $[\text{tfa}]^-$ ions.

FULL PAPER

MS/MS analyses on $[\text{Mn}(\text{hfa})_3]^-$ ions yielded the sole hfa^- (see Figure S7 in the Supporting Information), in line with previous results obtained in the ESI-MS analysis of $\text{Fe}(\text{hfa})_2 \cdot \text{TMEDA}$.^[15a] The different behavior of the two complexes emerging from Figure 5 suggested a different binding capacity of hfa and tfa ligands towards $\text{Mn}(\text{II})$ center. Indeed, both $[\text{MnL}_3]^-$ adducts were predicted to be stable with respect to the separated L^- and MnL_2 fragments, but the calculated formation energies differ by $2.0 \text{ kcal} \cdot \text{mol}^{-1}$ in methanol ($7.4 \text{ kcal} \cdot \text{mol}^{-1}$ in vacuum) in favor of $[\text{Mn}(\text{hfa})_3]^-$ (see Figure S8 in the Supporting Information). Furthermore, since the formation of $[\text{MnL}_3]^-$ adducts would involve the fragmentation of at least two $\text{MnL}_2 \cdot \text{TMEDA}$ molecules, it might be argued that the higher $\text{Mn}(\text{hfa})_2 \cdot \text{TMEDA}$ dipole moment could promote a head-to-tail alignment of two such molecules, enhancing the probability of a successful TMEDA/ hfa ligand exchange leading to the observed anion. Finally, it is worth noticing that no dimer/polynuclear species have ever been detected. Considering the ESI-MS soft ionization conditions, this result suggests that both complexes are monomeric, in tune with structural analyses (see above).

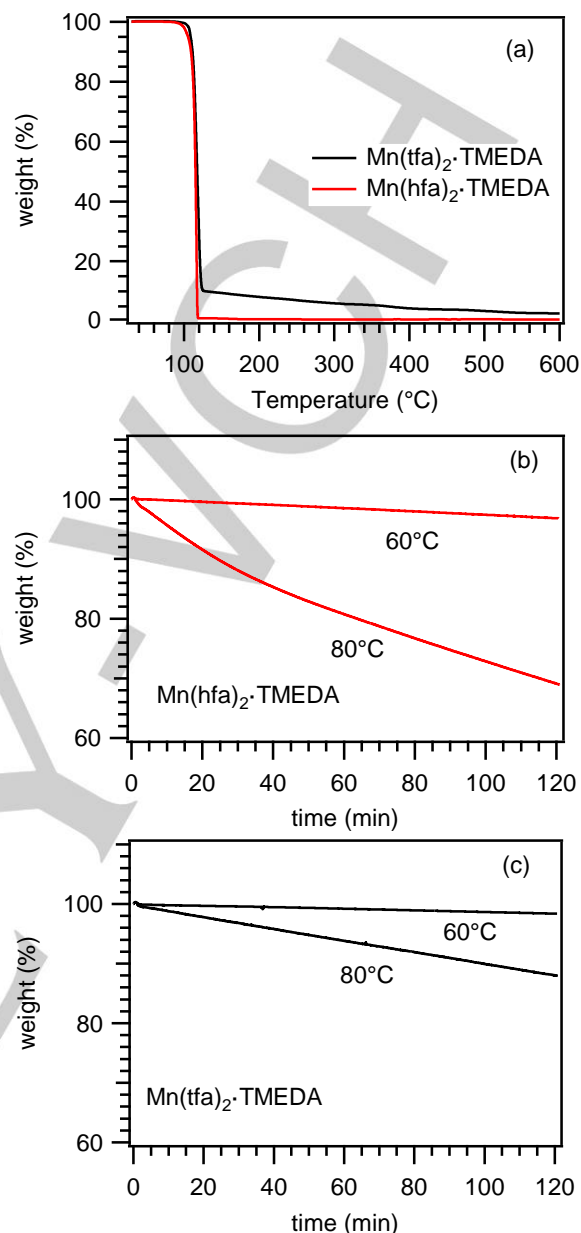


Figure 6. (a) TGA profiles for $\text{MnL}_2 \cdot \text{TMEDA}$ complexes. Isothermal weight changes recorded for: (b) $\text{Mn}(\text{hfa})_2 \cdot \text{TMEDA}$; (c) $\text{Mn}(\text{tfa})_2 \cdot \text{TMEDA}$.

To be successfully employed as CVD/ALD precursors, the target compounds should possess sufficient stability to ensure a vaporization free from undesired side decomposition, as well as a constant and reproducible vapor supply. To investigate the precursor thermal properties as a function of the ligand nature, thermogravimetric (TGA) analyses were performed for both $\text{MnL}_2 \cdot \text{TMEDA}$ compounds, yielding very similar results for freshly synthesized and aged sample batches. As can be observed in Figure 6a, both the target adducts displayed a similar behavior, characterized by a single-step mass loss for $T \geq 120^\circ\text{C}$, indicating a high volatility. As concerns $\text{Mn}(\text{hfa})_2 \cdot \text{TMEDA}$, the residual weight was close to zero for $T \geq 150^\circ\text{C}$, evidencing the occurrence of a

FULL PAPER

clean and quantitative vaporization in a narrow temperature range. The latter phenomenon is a key advantage in view of CVD/ALD applications, especially if compared with commonly used Mn precursors, that show either a lower volatility [as observed for $\text{Mn}(\text{dpm})_3$, with $\text{dpm} = 2,2,6,6\text{-tetramethyl-}3,5\text{-heptanedionate}$] or multi-stage decompositions, with a high residual weight [as observed for $\text{Mn}(\text{acac})_2(\text{H}_2\text{O})_2$, where $\text{acac} = 2,4\text{-pentanedionate}$].^[10c,11] Differential scanning calorimetry (DSC) analyses (not reported) enabled to identify the presence of two endothermic peaks at 84.5 and 100.6°C for $\text{Mn}(\text{hfa})_2\cdot\text{TMEDA}$ and $\text{Mn}(\text{tfa})_2\cdot\text{TMEDA}$, respectively, related to melting processes. In line with melting point values, $\text{Mn}(\text{tfa})_2\cdot\text{TMEDA}$ presented a slightly higher volatilization onset than $\text{Mn}(\text{hfa})_2\cdot\text{TMEDA}$, in line with the lower fluorine content of the former compound (see above).^[10d] In addition, a non-zero residual weight, progressively lowering from 130 to 600°C, could be observed.

Isothermal analyses (Figures 6b-c) carried out for 2 h evidenced a nearly constant weight loss as a function of time for both compounds. Such results, in line with previous reports on Fe, Co and Cu hfa derivatives,^[13,15a] enabled to rule out detrimental decomposition phenomena and confirmed the occurrence of a clean vaporization, an important feature for CVD/ALD applications.

CVD depositions from $\text{MnL}_2\cdot\text{TMEDA}$

An important point of this study has been the functional validation of $\text{MnL}_2\cdot\text{TMEDA}$ compounds, in order to assess their potential as CVD precursors for the fabrication of manganese oxide nanosystems. Preliminary deposition experiments were carried out on both Si(100) and SiO_2 substrates, using vaporization temperature ($\leq 65^\circ\text{C}$) and growth temperatures (400°C) lower than those previously adopted in vapor phase processes from conventional manganese precursors, such as $\text{Mn}(\text{hfa})_2$ and $\text{Mn}(\text{dpm})_3$, and also from $\text{Mn}(\text{hfa})_2\cdot\text{TMEDA}$.^[1e,10a,b,10e,11,17] The obtained brownish samples, characterized by a good adhesion with the substrate, were preliminarily investigated by X-ray diffraction (XRD, Figure 7), which revealed the formation of body-centered tetragonal Mn_3O_4 [*hausmannite*; space group: $I4_1/amd$;^[1a,2a,32] lattice parameters $a = 5.762 \text{ \AA}$, $c = 9.470 \text{ \AA}$; average crystallite size = $(40 \pm 5) \text{ nm}$], with Mn(III) and Mn(II) centers in octahedral and tetrahedral sites, respectively^[2b,5b,7] (Figure 7, inset). Irrespective of the used substrate, no reflections related to other Mn oxides or Mn(II) fluoride could be detected, indicating the obtainment of phase-pure systems, as also confirmed by X-ray photoelectron spectroscopy (XPS; see Figure S9 in the Supporting Information). The system morphology, analyzed by means of field emission-scanning electron microscopy (FE-SEM, Figures 8a-b), revealed the presence of well interconnected lamellar structures [average dimensions = $(270 \pm 50) \text{ nm}$] uniformly distributed over the substrate surface. From the mean nanodeposit thickness [$(350 \pm 20) \text{ nm}$], an average growth rate of $6 \text{ nm} \times \text{min}^{-1}$ could be estimated.

The compositional purity of Mn_3O_4 systems was confirmed by energy dispersive X-ray spectroscopy (EDXS) analysis. The obtained spectrum (Figure 8c) showed the presence of $\text{MnK}\alpha$ and

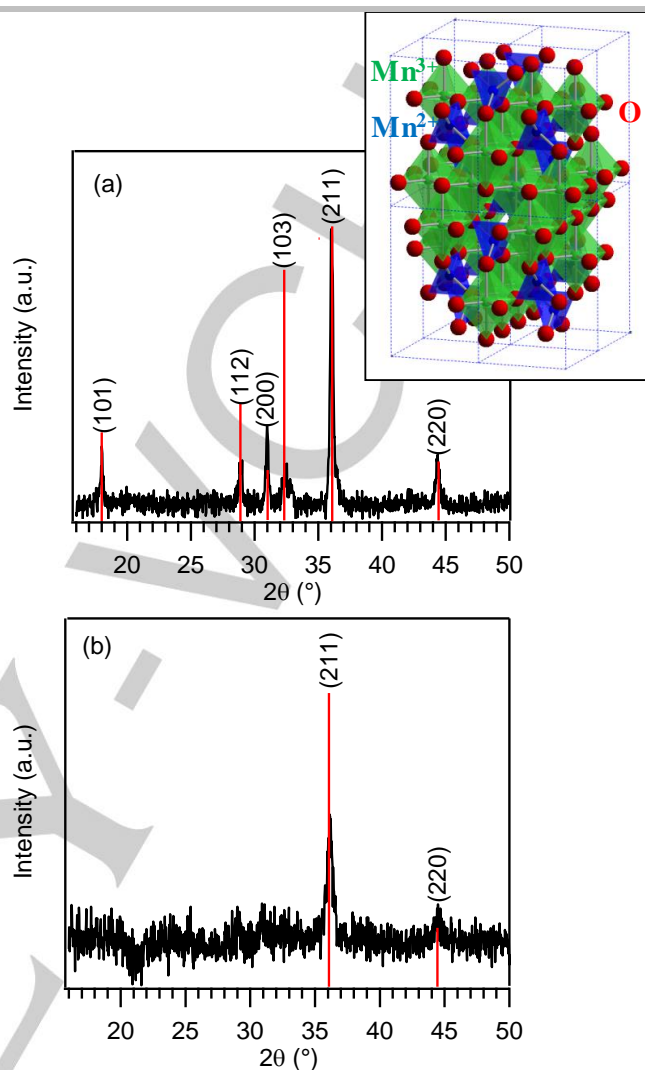


Figure 7. Glancing angle XRD patterns of Mn_3O_4 systems deposited at 400°C: a) on Si(100), from $\text{Mn}(\text{hfa})_2\cdot\text{TMEDA}$; b) on SiO_2 , from $\text{Mn}(\text{tfa})_2\cdot\text{TMEDA}$. Vertical bars mark the relative intensities of Mn_3O_4 powder spectrum. Inset: representation of the Mn_3O_4 solid state structure.^[32]

$\text{MnK}\beta$ peaks located at 5.90 and 6.50 keV, as well as the $\text{OK}\alpha$ signal at 0.52 keV. No evidences of C or F presence could be detected, in agreement with the clean precursor decomposition discussed above. Irrespective of the analyzed region, in-plane EDXS analyses highlighted a homogeneous oxygen and manganese lateral distribution.

Efforts were also devoted to the characterization of systems supported on silica. To this regard, the surface morphology was investigated by atomic force microscopy (AFM) (Figures 9a-b), that showed the presence of well interconnected protruding nanograins. The deposit appeared homogeneous and free from cracks/pinholes. From the line height profile, a root mean square (RMS) roughness of 5 nm could be evaluated.

Finally, optical absorption analyses were carried out (Figure 9c). The spectral shape was in line with that reported for Mn_3O_4 -based materials.^[4] As can be observed, the system was almost transparent in the IR range, whereas the significant absorption at

FULL PAPER

lower wavelengths ($\lambda < 600$ nm) corresponded to interband transitions. The optical band gap was estimated by the Tauc method, plotting $(\alpha h\nu)^n$ vs. $h\nu$ (Figure 9c, inset), with $n = 2$ corresponding to direct allowed transitions,^[1d,33] and extrapolating the obtained trend to zero absorption. The estimated value ($E_G = 2.5$ eV) was in line with previous literature data for Mn_3O_4 ,^[4-5] and highlighted the efficient harvesting of Vis light, paving the way to the use of the developed materials in solar-assisted applications.

Conclusions

The present work was devoted to the preparation and joint experimental/theoretical characterization of two different Mn(II) diamine diketonate adducts, of interest as molecular precursors for the vapor deposition of Mn oxide nanomaterials. The target molecular systems, $Mn(hfa)_2 \cdot TMEDA$ and $Mn(tfa)_2 \cdot TMEDA$, designed as alternatives to the well-known manganese β -diketonates, differ for the presence of one $-CF_3$ group in the ligand chain. The two compounds, developed by a simpler route than that previously reported for $Mn(hfa)_2 \cdot TMEDA$, are monomeric and water-free, thanks to the complete saturation of Mn(II) coordination environment. In particular, F presence in the diketonate moieties plays a key role in the complexes stabilization and in the obtainment of chemico-physical properties (thermal behavior and gas-phase reactivity) favorable for CVD/ALD applications.

The present results highlight that variations in the fluorine content of β -diketonate ligands does not affect appreciably the stability to air and moisture of these precursors. The differences in the

behavior of the two compounds, highlighted by ESI fragmentation patterns, could mainly be related to the different charge distribution in their molecular structures depending on the nature of β -diketonate ligand. Both precursors exhibit a higher volatility than conventional Mn β -diketonates, paving the way to their successful application for the vapor phase deposition of Mn oxides. Preliminary CVD experiments enabled the preparation of high purity, single-phase Mn_3O_4 nanomaterials endowed with tailored morphology, as well as an appreciable Vis light absorption. These results candidate the developed nanosystems for possible technological end-uses in solar driven processes, ranging from photoactivated H_2O splitting to wastewater purification, as well as in the development of solid state gas sensing devices for the detection of toxic/flammable analytes (such as CO , CH_4 ,...). Additional attractive perspectives for the prosecution of this work will involve the thorough use of both molecular compounds in CVD/ALD processes, to explore in detail the interplay between processing parameters and the resulting material properties. Preliminary studies in these research areas are actually being carried out within our group.

Experimental Section

General procedures

$MnCl_2 \cdot 4H_2O$ (98+%), $Hhfa$ (98%) and $Htfa$ (98%) were purchased from Strem Chemicals® and $TMEDA$ ($\geq 98\%$) from Merck®, all were used without further purification. All manipulations were carried out under normal laboratory conditions. The complex melting points (m.p.) were measured in

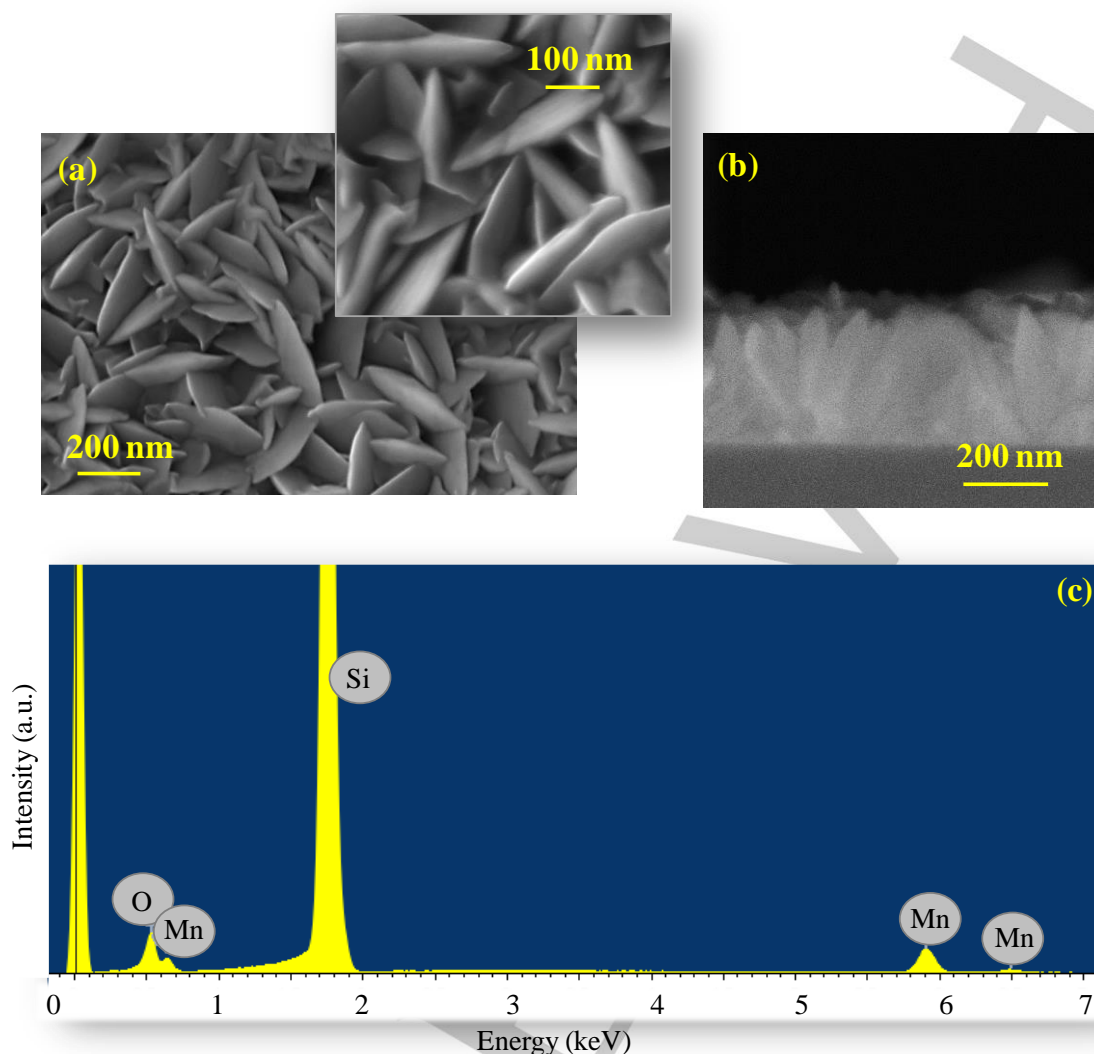


Figure 8. (a) Plane-view and (b) cross-sectional FE-SEM micrographs of a Mn_3O_4 specimen deposited on Si(100) at 400°C from $\text{Mn}(\text{hfa})_2\cdot\text{TMEDA}$. (c) Corresponding EDXS spectrum.

air by a FALC melting point device at atmospheric pressure. Elemental analyses were carried out by a Fisons Carlo Erba EA1108 apparatus (CHNS version).

Synthesis of $\text{Mn}(\text{hfa})_2\cdot\text{TMEDA}$

The synthesis of the target adduct was performed following a different procedure with respect to that previously reported.^[11,17] To a stirred aqueous solution of $\text{MnCl}_2\cdot 4\text{H}_2\text{O}$ (2.37 g, 11.73 mmol, in 50 mL of deionized H_2O) were slowly added 3.4 mL of Hhfa ($d = 1.47 \text{ g}\cdot\text{mL}^{-1}$, 23.30 mmol). The subsequent dropwise addition of NaOH (0.93 g, 23.50 mmol, in 10 mL deionized H_2O) yielded a clear yellow solution. 1.9 mL of TMEDA ($d = 0.78 \text{ g}\cdot\text{mL}^{-1}$, 12.59 mmol) were then slowly added to the reaction mixture, that turned to a maroon-like color. After reacting for 150 min in the dark, the obtained product was repeatedly extracted in dichloromethane up to the obtainment of a completely colorless aqueous phase. The organic solution was thoroughly washed with deionized water and the solvent was removed at room temperature under reduced pressure ($\approx 10^{-3}$ mbar), ultimately affording a yellow-orange solid. Yield: 5.15 g (75%); m.p. = 86°C at 1 atm;

elemental analysis calcd. (%) for $\text{C}_{16}\text{H}_{18}\text{O}_4\text{N}_2\text{F}_{12}\text{Mn}$ ($M_w = 585.25$): C 32.84, H 3.10, N 4.79; found: C, 33.60; H, 2.90; N, 4.78.

Synthesis of $\text{Mn}(\text{tfa})_2\cdot\text{TMEDA}$

To an aqueous solution of $\text{MnCl}_2\cdot 4\text{H}_2\text{O}$ (2.37 g, 11.73 mmol, in 50 mL of deionized H_2O), maintained under vigorous stirring, were slowly added 2.9 mL of Htfa ($d = 1.27 \text{ g}\cdot\text{mL}^{-1}$, 23.30 mmol), resulting in a phase separation. Subsequently, an NaOH solution (0.93 g, 23.50 mmol, in 10 mL deionized H_2O) was added dropwise, resulting in the formation of a yellow solution. 1.9 mL of TMEDA ($d = 0.78 \text{ g}\cdot\text{mL}^{-1}$, 12.59 mmol) were then added to the reaction mixture, which became maroon-like. After reaction in the dark for 150 min, the obtained product was repeatedly extracted in dichloromethane until the aqueous phase turned colorless. The organic solution was washed with deionized water and the solvent removed at room temperature ($\approx 10^{-3}$ mbar), yielding a light yellow solid. Yield: 3.7 g (66%); m.p. = 99°C at 1 atm; elemental analysis calcd (%) for $\text{C}_{16}\text{H}_{24}\text{O}_4\text{N}_2\text{F}_6\text{Mn}$ ($M_w = 477.31$): C 40.26, H 5.07, N 5.87; found: C, 40.93; H, 5.10; N, 6.03. Both $\text{Mn}(\text{hfa})_2\cdot\text{TMEDA}$ and $\text{Mn}(\text{tfa})_2\cdot\text{TMEDA}$ were stored at room temperature and could be easily handled in air without any detrimental

FULL PAPER

degradation. The powders were soluble in various solvents, such as hexane, dichloromethane, acetone and alcohols. In both cases, crystals for

X-ray analysis were obtained by re-dissolution in 1,2-dichloroethane, followed by slow solvent evaporation.

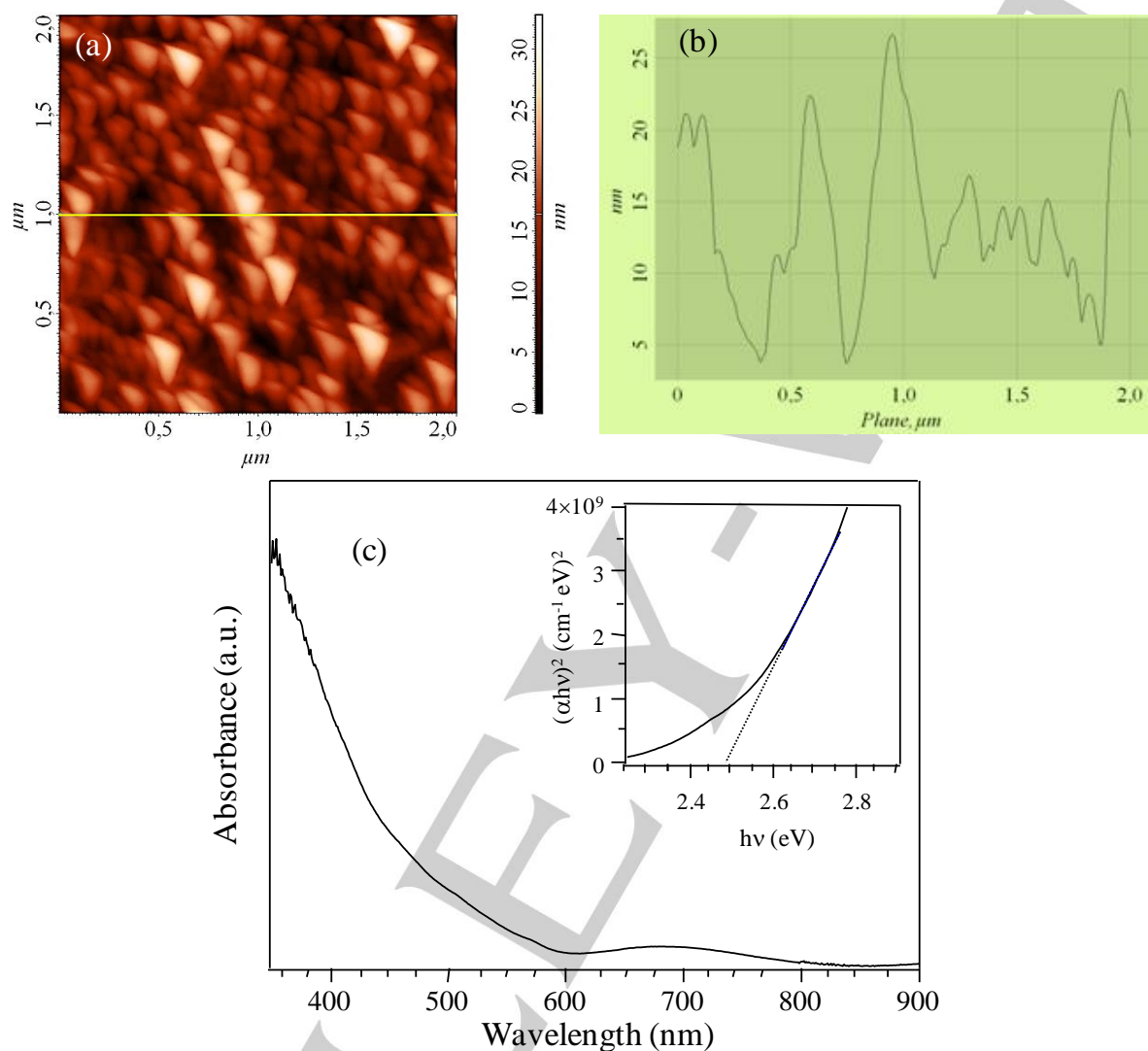


Figure 9. (a). Representative AFM image; (b) height profile along the marked line, and (c) optical spectrum and derived Tauc plot for a Mn_3O_4 deposit obtained on SiO_2 at 400°C from $\text{Mn}(\text{hfa})_2\cdot\text{TMEDA}$.

X-ray crystallography

Despite the structure of $\text{Mn}(\text{hfa})_2\cdot\text{TMEDA}$ has been previously reported,^[17] in this work crystallographic data were collected on both $\text{MnL}_2\cdot\text{TMEDA}$ compounds. In fact, since in the present work the compound $\text{Mn}(\text{hfa})_2\cdot\text{TMEDA}$ was prepared through a synthesis procedure different from that reported,^[17] a first aim was to verify the possible formation of different $\text{Mn}(\text{hfa})_2\cdot\text{TMEDA}$ polymorphs as a function of the adopted preparation route, as observed in the case of $\text{Cu}(\text{hfa})_2\cdot\text{TMEDA}$.^[13a] In addition, a key goal of this work was a detailed investigation of similarities and differences in the properties and behavior of $\text{MnL}_2\cdot\text{TMEDA}$ as a function of the ligand fluorination degree. Since the structure of $\text{Mn}(\text{hfa})_2\cdot\text{TMEDA}$ has never been reported so far, the investigation of the molecular structures of both compounds under the same experimental conditions and with a similar refinement quality was performed with the aim of attaining a direct and fine comparison of experimental data

pertaining to the two molecular systems. Furthermore, the simulation of compound properties, involving the electronic excitations analysis, the geometries of ions arising from their fragmentation, as well as the determination of their spin states, requires as a first step the optimization of the compound geometry, which, in turn, is based on the availability of structural data with similar quality in order to compare and validate the results obtained by computational experiments.

X-ray diffraction data for the synthesized compounds were collected on an Agilent Technologies SuperNova diffractometer with an Atlas CCD detector, using $\text{CuK}\alpha$ radiation ($\lambda = 1.54184 \text{ \AA}$) from multilayer X-ray optics. The crystals were coated with a perfluoropolyether, picked up with a glass fiber, and mounted in the nitrogen cold gas stream of the diffractometer. The obtained data were processed with CrysAlisPro.^[34] An absorption correction based on multiple-scanned reflections was carried out with ABSPACK in CrysAlisPro. The crystal structure was solved by direct

methods using SHELXS-97 and refined with SHELXL-2013.^[36] For Mn(hfa)₂•TMEDA, two of the CF₃ groups showed rotational disorder. Disordered parts were modeled with appropriate restraints and constraints on geometry and atomic displacement parameters (ADPs). Anisotropic ADPs were introduced for all non-hydrogen atoms. Hydrogen atoms were placed in geometrically calculated positions and refined with the appropriate riding model.

Analysis techniques

Optical spectroscopy analyses were carried out using a Cary 50 spectrophotometer (Varian; spectral bandwidth = 1 nm). Measurements were carried out on 10⁻⁶ M ethanol solutions of both Mn(hfa)₂•TMEDA and Mn(tfa)₂•TMEDA, using quartz cuvettes (optical path = 0.5 cm).

ESI-MS characterization was carried out using a LCQ Fleet ion trap instrument (ThermoFisher), operating in both positive and negative ion modes. The used entrance capillary temperature and voltage were set at 250°C and 4 kV, respectively. 10⁻⁶ M solutions of the target Mn compounds in methanol were introduced by direct infusion using a syringe pump (flow rate = 8 μL×min⁻¹). MSⁿ experiments were performed by applying a supplementary Radio Frequency (RF) voltage to the ion trap end caps (5 V peak-to-peak).

TGA analyses were performed with a TGA 2950 thermobalance manufactured by TA Instruments. Measurements were conducted under a pre-purified nitrogen atmosphere (heating rate = 10°C×min⁻¹) on samples which had a mass between 5 and 10 mg. DSC analyses were carried out using a MDSC2920 apparatus (TA Instruments) equipped with a liquid nitrogen cooling system using a heating rate of 3°C×min⁻¹.

Simulation

DFT calculations on Mn(hfa)₂•TMEDA and Mn(tfa)₂•TMEDA were performed with the PBE functional^[36] augmented with the long-range corrections of Hirao.^[37] Gaussian 09 was adopted,^[38] with Stuttgart-Dresden ECP pseudopotential for Mn and Stuttgart-Dresden basis set for all atoms.^[39] This basis set was enhanced with diffuse and polarization functions from the (D95++(d,p) basis set,^[40] which provided a satisfactory description of other members of the M(hfa)₂•TMEDA series.^[13a,14a,15a,b,16] All calculated minima had positive frequencies and were in the high-spin state (sextet). The spin state was established by optimizing the compounds geometry in the sextet, quartet and doublet states. Electronic excitations were calculated on the minimum energy structures by time-dependent (TD) DFT. The 50 excitations at lower energy were considered. The spectra reported in Figure 2b were obtained by smoothing the TD-DFT excitations with a 2 nm gaussian broadening. TD-DFT excitations were calculated for the two complexes also in ethanol, using a polarizable continuum model for the solvent.^[31] Natural Bond Orbitals (NBO) wavefunction analyses were performed with NBO 5.0.^[41] The compound decomposition energies (ΔE) with respect to the fragments take into account the zero-point-energy contributions and basis-set-superposition errors were counterpoise-corrected. Besides in vacuum, ΔE were calculated in methanol with a polarizable continuum model.^[31]

CVD synthesis and characterization of Mn₃O₄ nanomaterials

Manganese oxide depositions were performed by means of a custom-built cold-wall CVD reactor,^[15a] using Mn(hfa)₂•TMEDA and Mn(tfa)₂•TMEDA precursors contained in an external glass reservoir. In this study, the precursor vaporization temperatures were kept at 60°C and 65°C for Mn(hfa)₂•TMEDA and Mn(tfa)₂•TMEDA, respectively, while the substrate temperature was 400°C. Gas lines and valves connecting the precursor vessel and the reactor were maintained at T≥100°C for each growth process to prevent precursor condensation. Depositions were carried out in O₂-based atmosphere for 1 h on 1×1 cm² Si(100) (MEMC®, Merano, Italy) and Herasil silica (Heraeus®) substrates, which were subjected to

suitable pre-cleaning procedures before CVD experiments. For silicon substrates, the native SiO₂ layer was removed prior to deposition by means of HF etching. O₂ [total flow rate = 200 standard cubic centimetres per minute (sccm)] was used as carrier and reaction gas. Mass flow rates were controlled by MKS flow meters (Andover, Usa). The total pressure, measured by a capacitance manometer (BOC Edwards, Crawley, UK) was set at 10.0 mbar.

XRD patterns were recorded in glancing incidence mode (1°) on a Bruker D8 Advance X-ray diffractometer, equipped with a CuKα X-ray source (40 kV, 40 mA) and a Göbel mirror. Crystallite dimensions were estimated by the Scherrer equation.

FE-SEM analyses were performed by a Zeiss SUPRA 40 VP instrument, equipped with an Oxford INCA x-sight X-ray detector for EDXS investigation (primary beam voltage = 20 kV).

Optical absorption spectra for samples deposited on silica substrates were collected in transmission mode at normal incidence by means of a Cary 50 spectrophotometer, subtracting the substrate contribution. Tauc plots based on the obtained data were used to determine the optical band gap. AFM measurements were performed by a NT-MDT SPM solver P47H-PRO apparatus, operating in tapping mode. RMS roughness values were obtained from the analysis of 2×2 μm² images after plane fitting.

Acknowledgements

The authors kindly acknowledge the financial support under Padova University ex-60% 2014–2017, Insubria University FAR 2015-2016, P-DiSC #SENSATIONAL BIRD2016-UNIPD projects and ACTION post-doc fellowship. Thanks are also due to Mr. Loris Calore and to Mr. Filippo Gi (Padova University) for elemental microanalyses and useful experimental assistance.

Keywords: Mn β-diketonates • single-crystal X-ray diffraction • chemical vapor deposition • manganese oxides • nanomaterials

[1] a) Z. Chen, Z. Jiao, D. Pan, Z. Li, M. Wu, C.-H. Shek, C. M. L. Wu, J. K. L. Lai, *Chem. Rev.* **2012**, *112*, 3833-3855; b) Z. Bai, B. Sun, N. Fan, Z. Ju, M. Li, L. Xu, Y. Qian, *Chem. Eur. J.* **2012**, *18*, 5319-5324; c) E. Frey, P. Kurz, *Chem. Eur. J.* **2015**, *21*, 14958-14968; d) L. Ben Said, A. Inoubli, B. Bouricha, M. Amlouk, *Spectrochim. Acta, Part A* **2017**, *171*, 487-498; e) O. Nilsen, H. Fjellvåg, A. Kjekshus, *Thin Solid Films* **2003**, *444*, 44-51.

[2] a) Z.-Y. Fei, B. Sun, L. Zhao, W.-J. Ji, C.-T. Au, *Chem. Eur. J.* **2013**, *19*, 6480-6487; b) K. Wang, X. Ma, Z. Zhang, M. Zheng, Z. Geng, Z. Wang, *Chem. Eur. J.* **2013**, *19*, 7084-7089; c) D. M. Robinson, Y. B. Go, M. Mui, G. Gardner, Z. J. Zhang, D. Mastrogianni, E. Garfunkel, J. Li, M. Greenblatt, G. C. Dismukes, *J. Am. Chem. Soc.* **2013**, *135*, 3494-3501.

[3] M.-K. Song, S. Cheng, H. Chen, W. Qin, K.-W. Nam, S. Xu, X.-Q. Yang, A. Bongiorno, J. Lee, J. Bai, T. A. Tyson, J. Cho, M. Liu, *Nano Lett.* **2012**, *12*, 3483-3490.

[4] D. P. Dubal, D. S. Dhawale, R. R. Salunkhe, V. J. Fulari, C. D. Lokhande, *J. Alloys Compd.* **2010**, *497*, 166-170.

[5] a) D. P. Dubal, D. S. Dhawale, R. R. Salunkhe, S. M. Pawar, C. D. Lokhande, *Appl. Surf. Sci.* **2010**, *256*, 4411-4416; b) H. Y. Xu, S. Le Xu, X. D. Li, H. Wang, H. Yan, *Appl. Surf. Sci.* **2006**, *252*, 4091-4096.

[6] L. Zhang, Q. Zhou, Z. Liu, X. Hou, Y. Li, Y. Lv, *Chem. Mater.* **2009**, *21*, 5066-5071.

[7] H. W. Kim, Y. J. Kwon, H. G. Na, H. Y. Cho, C. Lee, J. H. Jung, *Microelectron. Eng.* **2015**, *139*, 60-69.

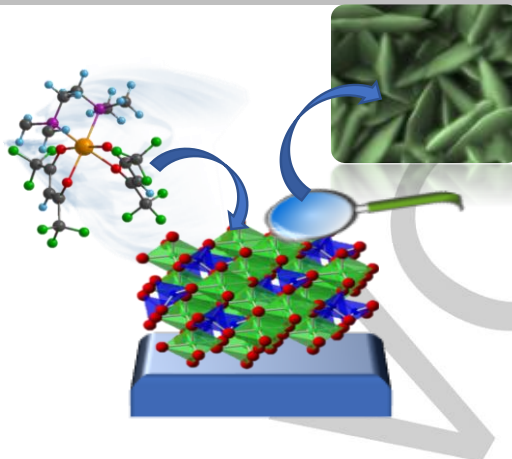
[8] a) H. Van Bui, F. Grillo, J. R. van Ommen, *Chem. Commun.* **2017**, *53*, 45-71; b) S. M. George, *Chem. Rev.* **2010**, *110*, 111-131; c) H.

- Pedersen, S. D. Elliott, *Theor. Chem. Acc.* **2014**, *133*, 1476; d) J. S. Price, P. Chadha, D. J. H. Emslie, *Organometallics* **2016**, *35*, 168-180.
- [9] a) A. Devi, *Coord. Chem. Rev.* **2013**, *257*, 3332-3384; b) P. Marchand, C. J. Carmalt, *Coord. Chem. Rev.* **2013**, *257*, 3202-3221; c) L. McElwee-White, *Dalton Trans.* **2006**, 5327-5333; d) C. E. Knapp, C. J. Carmalt, *Chem. Soc. Rev.* **2016**, *45*, 1036-1064; e) S. Mishra, S. Daniele, *Chem. Rev.* **2015**, *115*, 8379-8448.
- [10] a) T. Nakamura, *Phys. Status Solidi C* **2015**, *12*, 958-963; b) T. Nakamura, R. Tai, T. Nishimura, K. Tachibana, *J. Electrochem. Soc.* **2005**, *152*, C584-C587; c) S. Dhar, A. Varade, S. A. Shivashankar, *Bull. Mater. Sci.* **2011**, *34*, 11-18; d) S. I. Troyanov, O. Y. Gorbenko, A. A. Bosak, *Polyhedron* **1999**, *18*, 3505-3509; e) S. Kang, G. Brewer, K. R. Sapkota, I. L. Pegg, J. Philip, *IEEE Trans. Nanotechnol.* **2012**, *11*, 437-440.
- [11] Z. Lipani, M. R. Catalano, P. Rossi, P. Paoli, G. Malandrino, *Chem. Vap. Deposition* **2013**, *19*, 22-28.
- [12] A. R. Merritt, R. Rajagopalan, J. D. Carter, *Thin Solid Films* **2014**, *556*, 28-34.
- [13] a) G. Bandoli, D. Barreca, A. Gasparotto, R. Seraglia, E. Tondello, A. Devi, R. A. Fischer, M. Winter, E. Fois, A. Gamba, G. Tabacchi, *Phys. Chem. Chem. Phys.* **2009**, *11*, 5998-6007; b) G. Bandoli, D. Barreca, A. Gasparotto, C. Maccato, R. Seraglia, E. Tondello, A. Devi, R. A. Fischer, M. Winter, *Inorg. Chem.* **2009**, *48*, 82-89.
- [14] a) D. Barreca, E. Fois, A. Gasparotto, R. Seraglia, E. Tondello, G. Tabacchi, *Chem. Eur. J.* **2011**, *17*, 10864-10870; b) E. Fois, G. Tabacchi, D. Barreca, A. Gasparotto, E. Tondello, *Angew. Chem. Int. Ed.* **2010**, *49*, 1944-1948.
- [15] a) D. Barreca, G. Carraro, A. Devi, E. Fois, A. Gasparotto, R. Seraglia, C. Maccato, C. Sada, G. Tabacchi, E. Tondello, A. Venzo, M. Winter, *Dalton Trans.* **2012**, *41*, 149-155; b) D. Barreca, G. Carraro, A. Gasparotto, C. Maccato, R. Seraglia, G. Tabacchi, *Inorg. Chim. Acta* **2012**, *380*, 161-166; c) G. Tabacchi, E. Fois, D. Barreca, G. Carraro, A. Gasparotto, C. Maccato, in *Advanced Processing and Manufacturing Technologies for Nanostructured and Multifunctional Materials II*, John Wiley & Sons, Inc., **2015**, 83-90.
- [16] G. Tabacchi, E. Fois, D. Barreca, A. Gasparotto, *Phys. Status Solidi A* **2014**, *211*, 251-259.
- [17] G. Malandrino, R. G. Toro, M. R. Catalano, M. E. Fragalà, P. Rossi, P. Paoli, *Eur. J. Inorg. Chem.* **2012**, *2012*, 1021-1024.
- [18] F. A. Cotton, R. H. Holm, *J. Am. Chem. Soc.* **1960**, *82*, 2979-2983.
- [19] Y. Tohru, T. Toshihiro, R. Oliver, M. Teruaki, *Bull. Chem. Soc. Jpn.* **1991**, *64*, 2109-2117.
- [20] A. Lopez-Periago, O. Vallcorba, C. Frontera, C. Domingo, J. A. Ayllon, *Dalton Trans.* **2015**, *44*, 7548-7553.
- [21] N. A. Bailey, D. E. Fenton, M. V. Franklin, M. Hall, *J. Chem. Soc., Dalton Trans.* **1980**, 984-990.
- [22] W. B. S. McCormack, C.A., *UK Patent GB2022088A*, **1979**.
- [23] G. Tabacchi, E. Fois, D. Barreca, A. Gasparotto, *Int. J. Quantum Chem.* **2014**, *114*, 1-7.
- [24] B. S. Lim, A. Rahtu, J.-S. Park, R. G. Gordon, *Inorg. Chem.* **2003**, *42*, 7951-7958.
- [25] L.-Y. Wang, X.-Q. Wang, K. Jiang, J.-L. Chang, Y.-F. Wang, *J. Mol. Struct.* **2007**, *840*, 14-21.
- [26] F. H. Allen, *Acta Cryst.* **2002**, *B58*, 380-388.
- [27] H. Wang, Z. Liu, C. Liu, D. Zhang, Z. Lü, H. Geng, Z. Shuai, D. Zhu, *Inorg. Chem.* **2004**, *43*, 4091-4098.
- [28] D. Luneau, C. Stroh, J. Cano, R. Ziessel, *Inorg. Chem.* **2005**, *44*, 633-637.
- [29] J. Ni, H. Yan, A. Wang, Y. Yang, C. L. Stern, A. W. Metz, S. Jin, L. Wang, T. J. Marks, J. R. Ireland, C. R. Kannewurf, *J. Am. Chem. Soc.* **2005**, *127*, 5613-5624.
- [30] L. Wang, Y. Yang, J. Ni, C. L. Stern, T. J. Marks, *Chem. Mater.* **2005**, *17*, 5697-5704.
- [31] M. Cossi, V. Barone, B. Mennucci, J. Tomasi, *Chem. Phys. Lett.* **1998**, *286*, 253-260.
- [32] Pattern N° 024-0734, JCPDS (2000).
- [33] B. D. Viezbicke, S. Patel, B. E. Davis, D. P. Birnie, *Phys. Status Solidi B* **2015**, *252*, 1700-1710.
- [34] CrysAlisPro Software System, version 1.171.36.20; Agilent Technologies UK Ltd.: Oxford, U.K., 2012.
- [35] G. Sheldrick, *Acta Cryst.* **2008**, *A64*, 112-122.
- [36] J. P. Perdew, K. Burke, M. Ernzerhof, *Phys. Rev. Lett.* **1996**, *77*, 3865-3868.
- [37] a) H. Iikura, T. Tsuneda, T. Yanai, K. Hirao, *J. Chem. Phys.* **2001**, *115*, 3540-3544; b) A. W. Lange, M. A. Rohrdanz, J. M. Herbert, *J. Phys. Chem. B* **2008**, *112*, 6304-6308; c) J.-W. Song, T. Hirose, A. T. Tsuneda, K. Hirao, *J. Chem. Phys.* **2007**, *126*, 154105.
- [38] M. J. Frisch, G. W. Trucks, H. B. Schlegel, G. E. Scuseria, M. A. Robb, J. R. Cheeseman, J. A. Montgomery Jr., T. Vreven, K. N. Kudin, J. C. Burant, J. M. Millam, S. S. Iyengar, J. Tomasi, V. Barone, B. Mennucci, M. Cossi, G. Scalmani, N. Rega, G. A. Petersson, H. Nakatsuji, M. Hada, M. Ehara, K. Toyota, R. Fukuda, J. Hasegawa, M. Ishida, T. Nakajima, Y. Honda, N. O. Kitao, H. I. Klene, X. Li, J. E. Knox, H. P. Hratchian, J. B. Cross, V. Bakken, C. Adamo, J. Jaramillo, R. Gomperts, R. E. Stratmann, O. Yazyev, A. J. Austin, R. Cammi, C. Pomelli, J. Ochterski, P. Y. Ayala, K. Morokuma, G. A. Voth, P. Salvador, J. J. Dannenberg, V. G. Zakrzewski, S. Dapprich, A. D. Daniels, M. C. Strain, O. Farkas, D. K. Malick, A. D. Rabuck, K. Raghavachari, J. B. Foresman, J. V. Ortiz, Q. Cui, A. G. Baboul, S. Clifford, J. Cioslowski, B. B. Stefanov, G. Liu, A. Liashenko, P. Piskorz, I. Komaromi, R. L. Martin, D. J. Fox, T. Keith, M. A. Al-Laham, C. Y. Peng, A. Nanayakkara, M. Challacombe, P. M. W. Gill, B. G. Johnson, W. Chen, M. W. Wong, G. C., J. A. Pople, *GAUSSIAN 09 (Revision D.02)*, Gaussian, Inc., Wallingford, CT, **2009**.
- [39] A. Bergner, M. Dolg, W. Küchle, H. Stoll, H. Preuß, *Mol. Phys.* **1993**, *80*, 1431-1441.
- [40] T. H. Dunning Jr., P. J. Hay, in *Modern Theoretical Chemistry*, Plenum, New York, **1976**, Vol. 2, Chap. 1.
- [41] a) L. Goodman, R. R. Sauer, *J. Comput. Chem.* **2007**, *28*, 269-275; b) A. E. Reed, L. A. Curtiss, F. Weinhold, *Chem. Rev.* **1988**, *88*, 899-926; c) E. D. Glendening, J. K. Badenhop, A. E. Reed, J. E. Carpenter, J. A. Bohmann, C. M. Morales, F. Weinhold, in *NBO 5.0, Theoretical Chemistry Institute, University of Wisconsin, Madison, USA*, **2001**.

Entry for the Table of Contents

FULL PAPER

A convenient route for the synthesis of Mn(II) diamine diketonate complexes is proposed. For the first time, the target adducts are characterized in detail by a combined experimental-theoretical approach. The compounds possess a monomeric structure, very favorable mass transport properties and clean fragmentation, all of which make them promising precursors for the vapor phase fabrication of manganese oxide nanosystems.



Prof. Chiara Maccato, Dr. Lorenzo Bigiani, Dr. Giorgio Carraro, Prof. Alberto Gasparotto, Dr. Roberta Seraglia, Dr. Jiyeon Kim, Prof. Anjana Devi, Prof. Gloria Tabacchi, Prof. Ettore Fois, Dr. Giuseppe Pace, Prof. Vito Di Noto, and Dr. Davide Barreca

Molecular engineering of Mn(II) diamine diketonate precursors for the vapor deposition of manganese oxide nanostructures

WILEY-VCH